




## Original Article

# Tracking the spatiotemporal variability of the oxic–anoxic interface in the Baltic Sea with broadband acoustics

Elizabeth Weidner <sup>1,2,3\*</sup>, Christian Stranne<sup>2</sup>, Jonas Hentati Sundberg<sup>4</sup>, Thomas C. Weber<sup>3,5</sup>, Larry Mayer<sup>1,3</sup>, and Martin Jakobsson<sup>2</sup>

<sup>1</sup>Department of Earth Sciences, University of New Hampshire, Durham, NH, USA

<sup>2</sup>Department of Geological Sciences, Stockholm University, Stockholm, Sweden

<sup>3</sup>Center for Coastal and Ocean Mapping/Joint Hydrographic Center, University of New Hampshire, Durham, NH, USA

<sup>4</sup>Department of Aquatic Resources, Swedish University of Agricultural Sciences, Lysekil, Sweden

<sup>5</sup>Department of Mechanical Engineering, University of New Hampshire, Durham, NH, USA

\*Corresponding author: tel: +1 603 862 1581; e-mail: [eweidner@ccom.unh.edu](mailto:eweidner@ccom.unh.edu).

Weidner, E., Stranne, C., Sundberg, J. H., Weber, T. C., Mayer, L., and Jakobsson, M. Tracking the spatiotemporal variability of the oxic–anoxic interface in the Baltic Sea with broadband acoustics. – ICES Journal of Marine Science, 77: 2814–2824.

Received 6 March 2020; revised 24 July 2020; accepted 29 July 2020; advance access publication 3 November 2020.

Anoxic zones, regions of the water column completely devoid of dissolved oxygen, occur in open oceans and coastal zones worldwide. The Baltic Sea is characterized by strong salinity-driven stratification, maintained by occasional water inflows from the Danish Straights and freshwater input from rivers. Between inflow events, the stratification interface between surface and deep waters hinders mixing and ventilation of deep water; consequently, the bottom waters of large regions of the Baltic are anoxic. The onset of the anoxic zone is closely coincident with the depth of the halocline and, as a result, the interface between oxic and anoxic waters corresponds to a strong impedance contrast. Here, we track acoustic scattering from the impedance contrast utilizing a broadband split-beam echosounder in the Western Gotland Basin and link it to a dissolved oxygen level of 2 ml/l using ground truth stations. The broadband acoustic dataset provides the means to remotely observe the spatiotemporal variations in the oxic–anoxic interface, map out the extent of the anoxic zone with high resolution, and identify several mechanisms influencing the vertical distribution of oxygen in the water column. The method described here can be used to study other systems with applications in ongoing oceanographic monitoring programs.

**Keywords:** anoxia, Baltic Sea, broadband acoustics, climate change, coastal, hypoxia, stratification

## Introduction

Anoxic zones, regions of the water column completely devoid of dissolved oxygen, occur in open oceans and coastal zones worldwide (Diaz and Rosenberg, 2008). Formed as a result of an imbalance in transportation rates of organic matter and oxygen in deep waters, anoxic regions dramatically alter marine ecosystems (Conley *et al.*, 2009). As the climate warms many of the drivers of anoxic conditions are enhanced and, as a result, anoxic zones worldwide have expanded in recent decades (Stramma *et al.*, 2008) and are likely to grow larger in the near future. In this article, we identify and continuously track the anoxic zone in the

Western Gotland Basin of the Baltic Sea using a broadband acoustic method, providing a high-resolution map of anoxic waters that can be used for more accurate areal and volume extent estimates. Furthermore, the broadband data provide the means to discern local mixing dynamics and the mechanisms influencing the vertical distribution of oxygen in the water column, providing a pathway to deeper understanding of anoxic zone extent.

The Baltic Sea is a nearly landlocked marginal sea connected to the Atlantic Ocean through the Kattegat, Skagerrak, and North Sea. It is particularly prone to deep water anoxic conditions, due to a combination of limited water exchange through the narrow

and shallow Danish Straits and heavy freshwater and nutrient inflow from riverine sources (Winsor *et al.*, 2001; Conley *et al.*, 2002). The strong salinity-driven stratification and restricted water exchange through the Danish Straits prevents regular ventilation of deep water, resulting in relatively long residence times, on the order of 30 years (Döös *et al.*, 2004; Meier *et al.*, 2006). Consequentially, low oxygen conditions have frequented the Baltic Sea over the past thousand years (Andrén *et al.*, 2000; Zillén *et al.*, 2008). The present anoxic conditions in the Baltic Sea encompass between 12 000 and 70 000 km<sup>2</sup> (Carstensen *et al.*, 2014) and have resulted in water column habitat losses for major fisheries, such as Eastern Baltic Cod (Rabalais *et al.*, 2002; Casini *et al.*, 2016), the complete elimination of benthic faunal species (Vaquer-Sunyer and Duarte, 2008), and altered nutrient cycling (Mortimer, 1941; Smith and Hollibaugh, 1989).

Regular mapping of the spatial and volumetric extent of anoxic waters in the Baltic Sea has taken place since the early 1960s (Fonselius and Valderrama, 2003). These efforts utilize water column oxygen profiles measured *in situ* at discrete locations by ship-based or moored sensors (Carstensen *et al.*, 2014). These methods provide high-resolution vertical profiles of dissolved oxygen levels at the individual points of collection, but broad interpolation is required to create spatial maps to define the full extent and nature of the anoxic zone. The resulting maps (e.g. Viktorsson, 2017; Hansson *et al.*, 2018) have low horizontal resolution due to the sparse data collection across the Baltic Sea and are costly to produce due to the large amount of station time required to collect the data. Regardless, these direct measurement efforts have identified an increase in the spatial and volumetric extent of anoxic waters in many basins of the Baltic Sea over the past several decades (Zillén *et al.*, 2008; Carstensen *et al.*, 2014). Drivers of this expansion are hypothesized to include higher nutrient loads from anthropogenic sources (Conley *et al.*, 2009; Hong *et al.*, 2012), decreases in oxygenated inflows through the Danish Straits (Kabel *et al.*, 2012; Schmale *et al.*, 2016), and an increase in the temperature of surface waters and river load due to the warming climate (Graham, 2004; Rabalais *et al.*, 2009). However, the limited spatial resolution of single-point profiles cannot provide high-resolution information on the changing extent of anoxic waters, nor afford insight into the mechanisms controlling the short-term variability in the anoxic zone.

Active acoustics have been used for over a century to identify, track, and quantify phenomenon in the water column based on scattering from changes in density and/or sound speed, i.e. acoustic impedance contrasts (Hayes, 1924). The primary advantage of acoustics, over station-based sampling methods, is the near-synoptic collection of high-resolution spatial and temporal water column data over large regions. Acoustic applications to ocean sciences include identification of military targets (Clay and Medwin, 1977), fisheries and biological oceanography research (Simmonds and MacLennan, 2005), characterization of gas bubbles and oil droplets (Anderson, 1950; Merewether *et al.*, 1985; Camilli *et al.*, 2012; Weidner *et al.*, 2019), and observation of turbulence-induced ocean structure (Proni and Apel, 1975; Lavery *et al.*, 2003). Recent commercialization of broadband acoustic systems has allowed for the detection and study of weakly scattering stratification phenomenon including interfaces associated with pycnoclines and thermohaline staircases (Ross and Lavery, 2012; Stranne *et al.*, 2017) and the base of the surface mixed layer (Stranne *et al.*, 2018), where very small changes in

temperature ( $\sim 0.05^\circ\text{C}$ ) and salinity ( $\sim 0.015\text{ g/kg}$ ) are discernable.

In the Baltic Sea, the salinity-driven stratification interface between oxic and anoxic waters represents a region where density and sound speed rapidly increase from lower values in the oxic waters to higher in the anoxic waters. This increase corresponds to a strong acoustic impedance contrast. Here, we show that in the Western Gotland Basin, the stratification interface can be tracked with high vertical resolution using a broadband acoustic system; furthermore, by linking the acoustic data to a series of ground truth stations, we can show that the interface is near coincident with the hypoxic depth horizon [here defined as 2 ml/l (89.32 mmol/kg) dissolved oxygen] and therefore the commencement of the low oxygen zone in the Western Gotland Basin of the Baltic Sea. The result of this work is a high-resolution map of the areal extent of low oxygen conditions in the Western Gotland Basin study site, which provides the means to study the mechanisms responsible for the vertical distribution of oxygen in the water column.

## Methods

### Data collection

Data were collected on the *Research Vessel (RV) Electra* between 12 and 14 June 2018, northeast of Öland, Sweden's second largest island, in the Western Gotland Basin of the Baltic Sea. The survey area covered a region of  $\sim 1000\text{ km}^2$  and with 300 km of track line (Figure 1). The Gotland Basin is a region known for anoxic bottom waters and steep halocline at  $\sim 60\text{ m}$  depth (Elken *et al.*, 2006; Hansson *et al.*, 2018).

Broadband acoustic water column data were collected with a Simrad EK80 wideband transceiver (WBT) transmitting through a Simrad ES70C split-beam transducer with a  $7^\circ$  circular beam. All system parameters (i.e. transmit power, signal mode, pulse length) were kept constant during acquisition. The system was operated continuously during survey operations in broadband mode with a frequency range between 45 and 90 kHz, providing 45 kHz of bandwidth and a vertical range resolution of  $\sim 1.5\text{ cm}$ . The transmit power was set to 150 W, and the pulse length was set to 2.024 ms. The acoustic system was calibrated using a 38.1-mm tungsten-carbine sphere during operations on 12 June, following the well-documented procedure described in Demer *et al.* (2006).

Position and attitude data were collected and applied in real time from *RV Electra's* integrated Seapath 330+ GPS unit and MRU5+ motion sensor. The accuracy of horizontal and vertical positioning was  $\pm 0.5\text{ m}$  RMS. Pitch and roll accuracies were  $\pm 3\text{ cm}$  RMS for  $5^\circ$  amplitude. Heading accuracy was  $\pm 5\text{ cm}$  RMS for 4 m baseline (<http://www.km.kongsberg.com>).

Temperature, conductivity, and oxygen data were collected at 20 ground truth stations during survey operations using a Seabird SBE 9plus CTD (Conductivity, Temperature, Depth) unit, equipped with a Seabird SBE 43 oxygen sensor for dissolved oxygen profiles. The accuracies of the pressure, conductivity, temperature, and dissolved oxygen sensors are  $\pm 0.0015\%$  of full range ( $\sim 1400\text{ m}$ ),  $\pm 0.0003\text{ S/m}$ ,  $\pm 0.001^\circ\text{C}$ , and  $\pm 2\%$  of oxygen saturation, respectively ([www.seabird.com](http://www.seabird.com)).

During operations a weakly scattering interface was observed throughout the survey region between the depths of  $\sim 50$  and  $70\text{ m}$  (Figure 2). The scattering interface evolved along the survey track, as multiple layers merged, dispersed, split, and appeared. Biological scattering from fish and fish aggregations were abundant above the scattering interface, while below the interface there

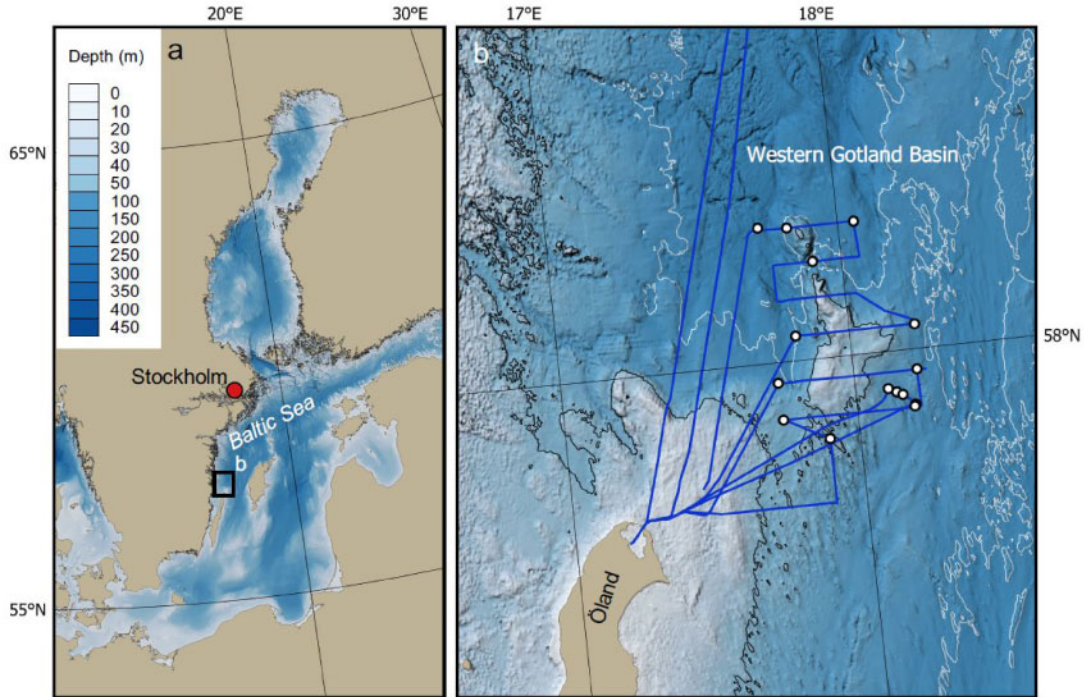


**Figure 1.** Overview image of the Baltic Sea (a). The inset in (b) shows the Western Gotland Basin and survey area. (b) The survey ship track lines (blue), and positions of ground truth stations (black encircled white dots) from survey operations. Bathymetry is from the digital bathymetric model by the European Marine Observation and Data Network (EMODnet Bathymetry Consortium, 2018).

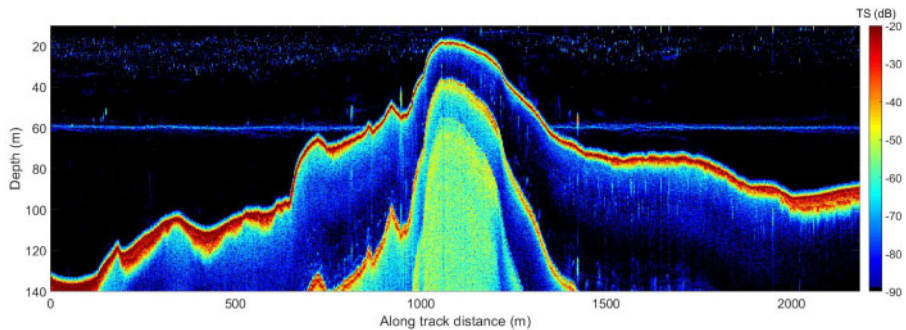


**Figure 2.** An example EK80 echogram showing scattering from the acoustic interface at ~60 m depth for >2 km.

was no indication of biological scattering in the water column. The depth of the scattering interface generally matches the previously reported coarsely mapped depth of the permanent halocline in the Western Gotland Basin (e.g. Elken *et al.*, 2006; Hansson *et al.*, 2018).

### CTD profile processing

CTD files were processed with the SBE data processing software, version 7.26.7 ([www.seabird.com](http://www.seabird.com)) and binned into 10 cm vertical averages. Using the binned data, temperature and salinity profiles were converted to absolute salinity and conservative temperature following the International Thermodynamic Equation of Seawater (IOC, SCOR and IAPSO, 2010) with the Gibbs-SeaWater (GSW) Oceanographic Toolbox for MATLAB 2017a (<http://www.teos-10.org/>). See [Supplementary data](#) for processed temperature and salinity profiles at all ground truth stations ([Supplementary Figures S1–S4](#)).

Following the procedure described in Stranne *et al.* (2017), an impedance ( $\eta$ ) profile was computed for each set of processed CTD data (Figure 3, see [Supplementary data S5–S8](#)) and from this, the reflection coefficient profile ( $R_{\text{CTD}}$ ) was estimated following:

$$R_{\text{CTD}}(i) = \frac{\eta(i) - \eta(i-1)}{\eta(i) + \eta(i-1)}, \quad (1)$$

where the  $i$ th element of  $R_{\text{CTD}}$  corresponds to the depth midway in between the depths  $z(i)$  and  $z(i-1)$  from the CTD profile data and  $\eta$  is the impedance at that depth as calculated from:

$$\eta(z) = \rho(z)c(z), \quad (2)$$

where  $\rho(z)$  is the density of seawater ( $\text{kg/m}^3$ ) and  $c(z)$  is the speed of sound in seawater (m/s), both computed from the processed CTD data.



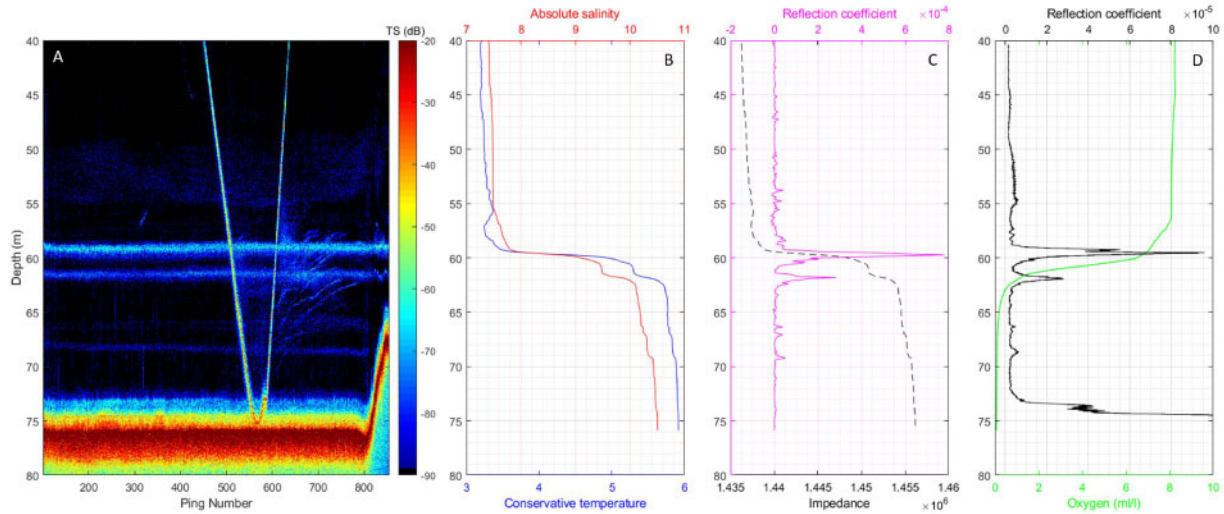


**Figure 3.** CTD and acoustic data from station 11. (a) An EK80 echogram from CTD station 11 showing several distinct horizontal bands of elevated scattering and the track of the CTD rosette traveling through the water column. (b) Processed profiles of temperature and salinity. (c) The impedance profile and the estimated reflection coefficients as derived from the CTD data. (d) The reflection coefficients as derived from EK80 data (black line) and plotted against the dissolved oxygen profile (green line).

Reflection coefficient profiles were computed at 16 of 20 CTD stations; stations 19 and 20 were in waters shallower than the halocline and stations 6 and 8 were used for a solar insolation experiments and did not contain a full water column profile.

### Acoustic water column data processing

All EK80 data were processed in MATLAB 2017a using a series of internal scripts and a software package provided by Kongsberg Maritime (L. Anderson, pers. commun.). A matched filter was applied to the acoustic water column data using an idealized replica signal. The high vertical range resolution of the match filtered broadband data allowed for the discrimination of acoustic scatterers in the water column at the sub-decimeter scale (see [Supplementary Figures S9–S12](#)). For all data, range from the transducer face was computed using the mean harmonic sound speed based on the nearest in time CTD profile. Range data were converted to depth by accounting for the static vessel draft and vessel heave.

A reflection coefficient profile was estimated from the processed EK80 data at all ground truth stations to compare against the CTD-derived reflection coefficient profile. The model that predicts acoustic backscattering at an interface assumes that the observed interface is a surface that extends beyond the ensonified area of the acoustic beam. Following [Stranne et al. \(2017\)](#), if the ensonifying acoustic pulse is assumed to be a plane wave, the calibrated acoustic backscattering ( $TS$ , target strength) from the layer can be predicted from the following:

$$TS(z) = 20 \log_{10} R_{EK80} + 10 \log_{10} A(r), \quad (3)$$

where  $R_{EK80}$  is the reflection coefficient and the area ensonified by the acoustic system at specific range,  $A(r)$ , can be computed from:

$$A(r) = \pi \left( r \times \tan \frac{\theta_{ES70}}{2} \right)^2, \quad (4)$$

where  $r$  is the range from transducer and  $\theta_{ES70}$  is the 3-dB circular beamwidth of the ES70 transducer.

This model is similar to the facet model for a rough seafloor, described in [Lurton \(2010\)](#), evaluated at normal incidence with unknown, but small slope variance and low distribution of slopes along the interface surface. The effects of interface roughness are ignored, as the depth of the scattering interfaces show very little variability ping-to-ping, with a root-mean-squared (RMS) height on the order of the range resolution (see [Figure 3](#) and [Supplementary Figures S9–S12](#)). This simplification likely introduced a small over estimation of the true reflection coefficient from the acoustic measurements, as roughness induces scattering of the incident wave at the interface, causing a loss of acoustic energy in the backscattered direction. However, the result does not affect our analysis and the simplification is in agreement with previous acoustic research on scattering from ocean pycnoclines ([Ross and Lavery, 2012](#)) and diffusive-convection interfaces ([Lavery and Ross, 2007](#)).

Using the measurements of  $TS$  computed from the processed EK80 data, (3) can be inverted to estimate the reflection coefficient from the scattering interface ( $R_{EK80}$ ). The acoustic reflection coefficient profile was computed using a running average filter, with a filter length of thirty-one acoustic profiles (acoustic system pings). All station data were collected while *RV Electra* was drifting and were sampled immediately before the CTD rosette passed through the scattering interface ([Figure 3](#)).

### Linking co-located water column profiles

The depth and magnitude of the maximum of the acoustically derived reflection coefficient profiles [ $R_{EK80}$  from (3)] were compared to the depth and magnitude of the maximum in the CTD-derived reflection coefficient profiles [ $R_{CTD}$  from (1)] (See [Supplementary Figures S13–S16](#)). In addition to direct comparison against the CTD reflection coefficient profiles, the frequency-modulated scattering response from the interface regions was explored in the EK80 dataset by taking a Fourier Transform of the calibrated acoustic time series. The resulting ensemble average spectra provided insight into the scattering mechanisms of the

observed interfaces. Finally, the position of the peak in the acoustically derived reflection coefficient profile was compared to the dissolved oxygen profile from the processed SBE43 unit data (Figures 3 and 4, see Supplementary Figures S17–S20). All analyses were limited to water column depths between 40 and 80 m, the region containing the permanent halocline and observed scattering interface.

### Oxic–anoxic interface tracking

The interface between oxic and anoxic waters was tracked based on the results from the ground truth CTD stations. The peak in the reflection coefficient profile, as derived from the processed EK80 acoustic water column data, was closely co-located to the hypoxic horizon in the water column. Before computing the reflection coefficient profile from the acoustic data for tracking purposes, several data masking steps had to be taken.

In regions where the scattering interface intersected with the seafloor (i.e. the depth of the seafloor approached ~50 m), the acoustic return from the seafloor was masked to prevent interference with the tracking algorithm. For each acoustic profile, the masking procedure identified the first instance of a *TS* measurement > -30 dB below 40 m depth, to avoid false seafloor detections due to fish in the upper water column. The index from this position was back-stepped by 300 samples, ~2 m of depth, to remove additional match filter-generated side-lobe interference. Data below the identified position were ignored in further calculations of the reflection coefficient profile.

In addition to intersections with the seafloor, in many instances, strong biological scattering, most likely aggregations of fish, were observed near to or in the scattering interface region. When present, scattering from fish dominates the acoustic record, making tracking the interface difficult. Fish aggregations were masked using a split-beam processing procedure known as the coherence factor (CF) index (Blomberg et al., 2018). The CF index provides a measurement of the data coherence measured across the elements of the EK80 receiver array at a single time point. CF is defined by the ratio of the coherent sum to incoherent sum of acoustic samples for the receiver elements, given by:

$$CF(p, r) = \frac{\sum_{m=1}^M y_m(p, r)^2}{M \sum_{m=1}^M y_m(p, r)^2}, \quad (\text{Eq. 5})$$

where for each receiver element  $m$ ,  $y_m$  denotes the match-filtered, complex valued sample at ping  $p$  and range  $r$ , and the total number of elements in the receiver is given by  $M$ . The EK80 split-beam transducer on *RV Electra* has four quadrants, so  $M = 4$  for this data set.

The CF index procedure allows for automated masking of most of the observed fish aggregations due to the difference between these aggregations and the interface layers. Scattering from randomly distributed organisms, as these aggregations appear to be, results in a combined scattered return that is incoherent across the split-beam receiver elements. By contrast, the interface layers, which are akin to surfaces that extend beyond the acoustic beam footprint, scatter sound coherently (Supplementary Figure S22). A CF index threshold of 0.4 was set and all data samples below the threshold were ignored in any further calculations of the reflection coefficient profile.

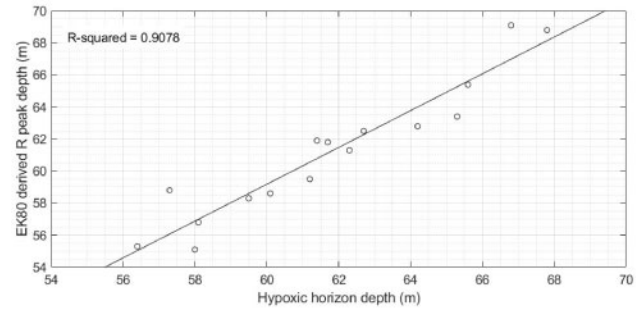


**Figure 4.** The depth of the hypoxic horizon, as calculated from the dissolved oxygen profiles, plotted against the depth of the peak in the acoustically derived reflection coefficient profile (circles) and the resulting linear regression of these data (solid line). The  $R$ -squared value of the regression is 0.9078.

The tracking procedure required that the acoustically derived reflection coefficient profile was computed for every ping along the *RV Electra*'s survey track. After the masking procedures were applied, the peak reflection coefficient for a given ping was computed from a running average filter with a filter length of 31 acoustic profiles. From the averaged reflection coefficient profile, the depth of the peak reflection coefficient in the water column was saved, as well as the latitude and longitude of the ping location. The tracking procedure was applied to all water column data between the depths of 40 and 80 m in the study area.

Maps detailing the spatial extent of the oxic–anoxic interface were created by interpolation between the measured depths from the highly resolved track derived from the acoustic algorithm (Figure 5). The interpolated maps were created in MATLAB using triangulation-based natural neighbor interpolation function onto a grid with 500 m  $\times$  500 m spacing, covering the survey region. Interpolated data were then masked in regions shallower than 50 m where the oxic–anoxic interface was not found due to shallow bathymetry.

## Results

### Linking co-located water column profiles

This analysis allows for direct comparison between the physical changes in the properties of the water column (e.g. the halocline) and the scattering observed at the acoustic scattering interface. Throughout the dataset, the two sets of derived reflection coefficient profiles show similar water column trends, as exemplified in Figure 3. The peaks in reflection coefficient profiles, which represent the position of the scattering interface, are co-located within a mean difference of  $1.0 \pm 1.3$  m standard deviation (Supplementary Table S1). Furthermore, the magnitude of the peak reflection values shows agreement between the two derivation methods. The relative error between peak magnitudes for a station is always within an order of magnitude, often much closer with a the mean relative error is 23.9% ( $\pm 16.2\%$ ) (Supplementary Table S2).

The spectra of the interfaces generally showed no frequency dependence, or in a few cases there was a very weak ( $k^{-1.2}$ ) frequency dependence (Supplementary Figure S21). Taken together with the comparison to the CTD reflection coefficient profiles, these findings suggest: (i) the smooth surface assumption is valid, as no frequency dependence would be expected, and (ii) scattering from the interface can be primarily explained the physical

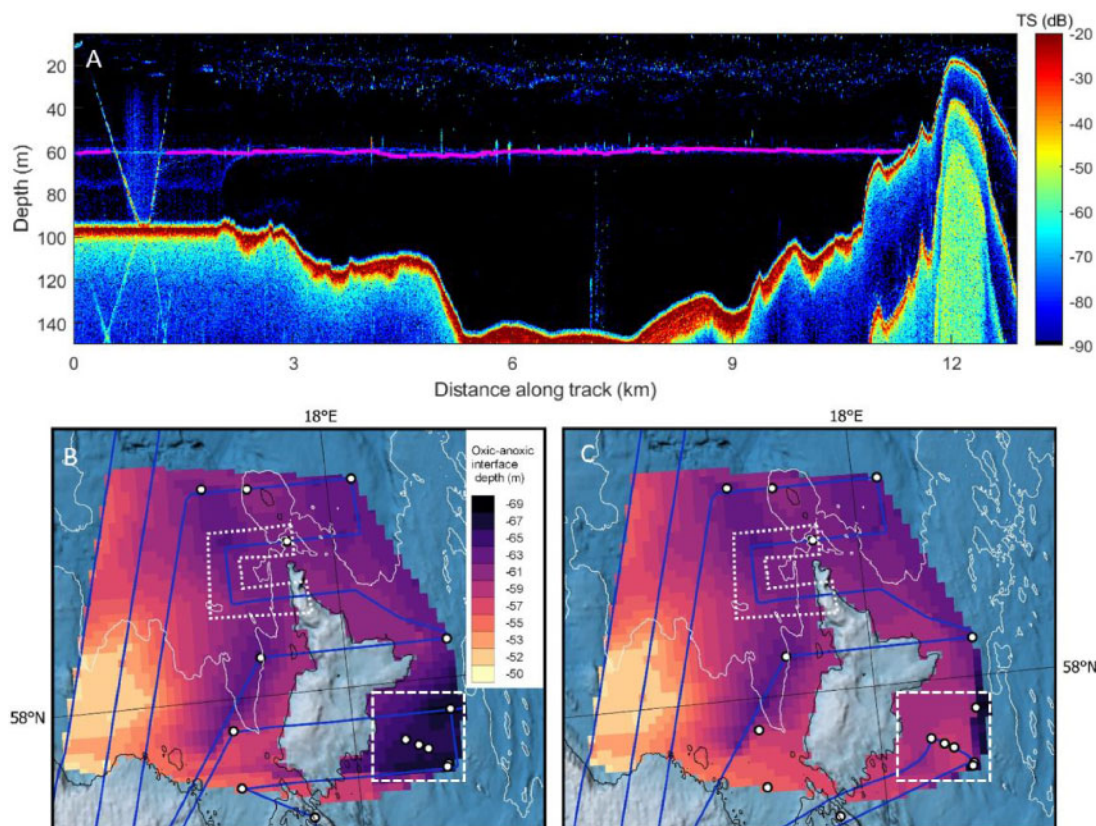


**Figure 5.** (a) An EK80 echogram transect of over 12 km starting at CTD station 13. The magenta line at ~60 m depth shows the result of interface tracking algorithm along the transit, which identifies the oxic–anoxic interface. (b and c) An overview map of the survey region with ship track lines (blue), CTD station locations (white markers with black outlines), and the results of the triangulation-based natural neighbor interpolation of the oxic–anoxic interface tracking algorithm. The interpolation map shown in (b) consist of data from 11, 13, 14, and 15 June. The panel (c) interpolation map consists of data from 11, 12, 13, and 15 June. Data from 12 and 14 June cover the same region, in the southeast corner of the survey area, and show significantly different interface depths (dashed box highlights this region). This is the results of suspected down-welling, which is discussed below. In addition, the position of the echogram from (a) is denoted with the dotted box in the middle of the interpolated maps.

**Table 1.** A comparison of the depth (in meters) of the peak reflection coefficient, as determined by the EK80 acoustic data inversion verse the depth of the point of hypoxia (2 ml/l dissolved oxygen) as measured by the oxygen sensor on the CTD.

Ground truth station ID	1	2	3	4	5	7	9	10	11	12	13	14	15	16	17	18
Depth (m)																
Hypoxic point	59.5	67.8	66.8	60.1	56.4	57.3	58.0	61.4	61.2	62.7	62.3	61.7	64.2	58.1	65.6	65.3
Peak EK80 derived R	58.3	68.8	69.1	58.6	55.3	58.8	55.1	61.9	59.5	62.5	61.3	61.8	62.8	56.8	65.4	63.4
Absolute difference (m)	1.2	1.0	2.3	1.5	1.1	1.5	2.9	0.5	1.7	0.2	1.0	0.1	1.4	1.3	0.2	1.9

changes in the water properties, as opposed to biology, turbulent microstructure, or some other scattering mechanism.

Throughout the ground truth station datasets the position of the peak reflection coefficient was closely located to the hypoxic oxygen horizon (2 ml/l dissolved oxygen) in the water column, often within <1 m (see Table 1). The minimum absolute different in depth was 0.1 m at station 14, the maximum was 2.9 m at station 9, and the mean difference was  $1.2 \pm 0.76$  m standard deviation. The results of linear regression between the datasets in Table 1 indicate strong correlation, with an  $R$ -squared value of  $>0.9$  (Figure 4). These results show that the position of the maximum reflection coefficient from the pycnocline region is not just within the oxycline, but closely associated with the hypoxic depth

horizon. By tracking the peak reflection coefficient from the acoustic dataset, we can track the hypoxic depth horizon in the water column to within ~1 m, which allows us to track the oxic–anoxic transition continuously over long distances using remote acoustic measurements.

### Oxic–anoxic interface tracking

The result of the oxic–anoxic interface tracking, shown in Figure 5 (top panel), is a highly resolved track, both vertically and horizontally, of the oxic–anoxic interface following Electra’s path across the Western Gotland Basin. The depth of the oxic–anoxic interface varies between 70 m at the deepest point and 49 m at the shallowest. The mean depth is  $62 \pm 4$  m, and there is a general



deepening of the interface from southwest to northeast across the survey site. The horizontal resolution is  $\sim 5$  m and is a function of the tracking algorithm averaging window and survey speed of *Electra*. The vertical resolution is  $\sim 1.5$  cm and is a function of the match-filtered range resolution of the EK80 system.

## Discussion

Anoxic zones, found in the Baltic Sea and throughout the world's oceans, affect nutrient cycling, carbon sequestration and biological productivity (Mortimer, 1941; Smith and Hollibaugh, 1989; Rabalais *et al.*, 2002; Vaquer-Sunyer and Duarte, 2008; Conley *et al.*, 2009; Casini *et al.*, 2016). The limited spatial resolution of traditional single-point oxygen profiles has hampered our ability to understand fine scale variations in the extent of anoxic waters; such measurements cannot provide high-resolution information on inter-seasonal timescale changes in the extent of anoxic waters, nor offer insight into the mechanisms controlling the short-term variability of the anoxic zone. In this article, we have identified and tracked the anoxic zone in the Western Gotland Basin using broadband acoustic methods, which afford high horizontal and vertical resolutions on the order of meters and centimeters, respectively.

### Patterns of oxie–anoxic interface across survey area

The anoxic zone of the Western Gotland Basin was mapped across the study area. There is an overall deepening of the oxie–anoxic interface from the southwest to the northeast of the survey site, generally following bathymetric trends in the region. The interface is at its shallowest as the acoustic track approached the shallow waters off the harbor on Öland; there, the interface intersected the seafloor at  $\sim 50$  m depth. Despite the overall deepening to the NE, the deepest measurement of the interface was  $\sim 70$  m depth, in the southeast corner of the survey site (Figure 5, dashed box). In the SE region, despite the short temporal scope of the study, we observed a strong temporal variation in the depth of the anoxic zone, with a deepening of  $>10$  m between the 12th and the 14th of June. We hypothesize that the dramatic change in depth of the interface in this region is related to a wind-driven event that will be discussed below. Overall, the interface showed lateral continuity over the survey area. In the central part of the survey area where the seafloor shallowed, the interface weakened and widened at the point of intersection with the seafloor (Supplementary Figure S23), potentially driven by near-boundary turbulence. During CTD operations, when *RV Electra* was drifting, internal waves were occasionally observed propagating along the scattering interface (see Supplementary Figures S10 and S11), although observations of internal waves were limited by the time at each station ( $<1$  hr). Observed wave amplitudes were on the scale of decimeters, and wave periods varied between  $\sim 130$  and 240 s.

As noted in the results, the depth of the oxie–anoxic interface as measured by the dissolved oxygen profiles at the ground truth stations agrees well with the acoustically derived results. A CTD-based interpolated map of the survey region would have shown an oxie–anoxic interface of relatively constant depth between  $\sim 60$  and 62 m, which agrees with previously published literature (Hansson *et al.*, 2018). However, it is clear from our interpolated maps that the discrete CTD stations fail to identify many of the details in the interface extent; specifically, the shallowest and deepest extents of the anoxic zone. These differences in resolution

and detail highlight the importance of using acoustic data as part of low-oxygen tracking and monitoring efforts. Furthermore, the spatial coverage of the ground truth stations is significantly less than that of the acoustic survey due to timing constraints during operations (see Figure 5). Although the acoustic tracking method depends on ground truth CTD data, running acoustic systems during all survey operations is inexpensive and efficient, providing spatial resolution orders of magnitude higher than that of CTD operations alone.

Previous work in the Western Gotland identified the permanent halocline at  $\sim 60$  m depth (Elken *et al.*, 2006; Hansson *et al.*, 2018). While our results generally agree with a mean depth of the halocline (and therefore oxie–anoxic interface) at  $\sim 60$  m, the variability in depth of the interface across the survey region is  $>20$  m. The higher resolution view of the oxie–anoxic interface provides the means to track changes and long-term variability in low-oxygen conditions via more accurate areal and volume extent estimates of the anoxic zone across the region, as well as the means to better study the processes controlling the extent of the anoxic zone, discussed below. It is important to note that there are limits to the interpretation of the interpolated maps shown in Figure 5. The acoustic data presented here were not collected as part of a regimented survey with equal spacing between track lines or any consideration of the track line density needed to capture the variability and spatial structure of the oxie–anoxic interface. The simple interpolation presented here suggests that structure in the spatial extent of the oxie–anoxic interface where there may be none does not consider the directional dependence of interface variability from currents or other oceanographic phenomenon and acts as only a first-order constraint on the depth of the anoxic zone. Furthermore, the data were collected in the beginning of the June and it is likely that seasonal processes, such as summer shallowing of the mixed layer, winter storm and wind events, or ice cover, may impact the depth and extent of the anoxic zone. Future, more regimented application of this method can provide a more complete picture of the extent of the oxie–anoxic interface by employing a higher density survey with equally spaced track lines and regimented CTD stations.

### Mechanisms controlling vertical profiles of dissolved oxygen distribution

The characteristics of the vertical dissolved oxygen profile in the Gotland Basin, and the broader Baltic Sea, are primarily defined by a permanent halocline, which is a function of the long-term balances between freshwater input from rivers and the sporadic inflows of dense, oxygenated water through the Danish Straits (Winsor *et al.*, 2001). In between major inflow events, during periods of deep-water stagnation, internal mixing processes influence the distribution of dissolved oxygen and other substances in the water column. These processes include wind-driven topographic waves, near-boundary turbulence, and double-diffusive convection (Holtermann *et al.*, 2017); however, the details of these processes and their magnitudes are not well understood and are the subject of ongoing research.

In the course of this research, we observed processes exerting vertical control over the dissolved oxygen level in the water column, specifically a wind-driven down-welling event and double diffusion-driven convection.

### Wind-driven down-welling

In the southeast corner of the survey site (see Figure 5), an apparent wind-driven down-welling event depressed the anoxic zone by ~10 m during the period of survey operations (Supplementary Figure S24). On 12 June 2018, *RV Electra* collected a series of ground truth stations (stations 4, 5, 7, and 9) and ~12.5-line kilometer of acoustic water column data. Both the ground truth stations and the acoustic tracking algorithm found the depth of the oxic–anoxic interface in this region to be  $58 \pm 1$  m, shallowing slightly to the south. Roughly 40 hr later on 14 June, *RV Electra* returned to the same region for another series of ground truth stations (stations 17 and 18) and acoustic data collection. During this data collection period, the depth of oxic–anoxic interface estimated by both datasets was  $67 \pm 1$  m, slightly deeper to the north.

The water column characteristics, as measured by the CTD profiles, show no indication of mixing between oxic and anoxic water masses between the period of the 12 and 14 June. Instead, the CTD profiles show slight freshening of surface water (depths <5 m) and downward depression of the water column in the region of the oxic–anoxic interface, suggesting a potential down-welling event.

No wind data were collected on *RV Electra* during this project, but wind magnitude and directional data were collected at a weather station operated by the Swedish Meteorological and Hydrological Institute, which was located at the nearby northern cape of Öland (number 77220, <https://www.smhi.se/data/meteorologi/vind>). Processing of this dataset shows a strong, sustained wind event on 12 June from 07:00 to 15:00, local time. During this period, winds with the magnitude of ~11 m/s blew from the southeast. Such an event could have caused a localized down-welling event to the southeast of the bathymetric high in the center of the survey region. Down-welling in this region would have shifted the water column downward, causing the depression of the oxic–anoxic interface that was observed during the acoustic data collection.

While the CTD casts from 12 and 14 June did capture the deepening of the halocline, the CTD data do not provide the same level of insight into the down-welling event as the acoustic data. The collection of the acoustic data expands the dimensionality of analysis including the possibility of determining the footprint of the deepening, allowing for study of the spatial variability and magnitude of change in the hypoxic horizon due to short-term events, as well as direct observation of the biological response. While the duration of data collection does not capture the full time period that this event will impact the anoxic zone, the down-welling event highlights the importance of using acoustic data to provide spatial context.

### Double-diffusive convection

Throughout the survey site the observed scattering interface evolved dramatically along the ship track, as multiple layers were seen merging, splitting, appearing and disappearing. Closer inspection of the CTD profiles revealed a double-diffusive convective mixing regime driven by the water column structure near the stratification interface with cold, fresher water sitting over denser warm, salty water (Supplementary Figure S25). In such situations, the difference in the diffusivities of heat and salt gives rise to step-like structures in the water column. These structures, often referred to as “thermohaline staircases”, have been well described in

the literature (e.g. Turner, 1968; Tait and Howe, 1968; Ruddick and Gargett, 2003) and observed in many regions (Timmermans *et al.*, 2008; Stranne *et al.*, 2017), including some parts of the Baltic Sea (Holtermann *et al.*, 2017; Umlauf *et al.*, 2018), although not in the Western Gotland Basin.

The staircases observed in the study site are characterized by one to three step features, with thicknesses between 0.5 and 2.0 m, salinity gradients 0.5–3.0 g/kg across interfaces, and temperature gradients 0.4–2.0°C across interfaces. The makeup of the staircases was not homogenous over the survey area; in some regions, staircases were well defined and discrete, while in others profiles there was a relatively smooth gradient between water masses with indications of not quite formed staircases, potentially representing the formation and/or deterioration of staircases. Heterogeneity of these features suggests the potential for different mixing rates across the survey area and, thus, different controls on the vertical profiles of dissolved oxygen.

Double-diffusive convective mixing is driven by potential energy from temperature gradients without the need for outside mechanical energy input. The majority of ocean thermohaline staircase phenomenon are low-energy systems, with slow and steady mixing, and heat flux rates on the order of 0.1 W/m<sup>2</sup> (Timmermans *et al.*, 2008; Shibley *et al.*, 2017); however, observations by Umlauf *et al.* (2018) in the Bornholm basin of the Baltic Sea describe rapidly forming staircases associated with fresh, cold intrusions and vertical heat fluxes on the order of 10 W/m<sup>2</sup>. This does not appear to be the case here, rather they appear to be associated with relatively stationary water column structure similar to those in the Arctic Ocean. Future broadband research will focus on determining the spatial variability of these staircase structures, estimating the rates of mixing associated with them, and studying their effect on the dissolved oxygen distribution in the Gotland Basin.

The identification of both the double diffusive convective mixing and the wind-driven down-welling highlights the need for regularly updated, high-resolution maps of the anoxic zone in the Baltic Sea. Short-term changes in the extent of the anoxic zone are likely not captured with traditional *in situ* discrete sampling methods, and while long-term trends may be observable, their impacts and effects might not be.

### Biological response to oxic–anoxic interface

As noted previously, there was abundant biological scattering in the survey area above the oxic–anoxic interface from individual fish, fish aggregations, and possibly zooplankton. This has been observed both in the Baltic and other low-oxygen regions (Eby and Crowder, 2002; Diaz and Rosenberg, 2008; Bertrand *et al.*, 2010). Strong biological scattering above the oxic–anoxic interface was ubiquitous across the survey region; however, the vertical distribution of observed scatterers was not homogenous. Throughout the survey region, in the shallow oxygenated water (depths <40 m), the observed biology was primarily composed of discrete targets. In deeper waters, close to the oxic–anoxic interface, scattering were observed from aggregations of many targets (e.g. groups of multiple fish in proximity). The fish aggregations were often found within <1 m of the point of hypoxia, suggesting a tolerance for low-oxygen conditions. The approach described here provides a series of measurements that can, at high-resolution, simultaneously identify biology and physical oceanographic properties, offering the opportunity for new levels of



understanding (e.g. fine-scale species interactions with the physical environment).

The observations of fish made in this study reinforce the results of prior research in the Baltic Sea that suggests that low-oxygen conditions are a major mechanism driving the vertical distribution of fish (Randell, 1970; Neuenfeldt, 2002). As the extent of the low oxygen waters grows, both laterally and vertically in the water column, the available habitat for fish in the Baltic Sea shrinks, highlighting the need for high-resolution maps of anoxic regions. The vertical separation of discrete fish targets and aggregations of fish to different depth regions supports the suggestion that the low-oxygen conditions are potentially de-coupling prey–predator interactions, (Taylor and Rand, 2003; Ekau *et al.*, 2010). The behavioral responses of fish species are complex and future research with this dataset will focus on quantifying the spatial relationship between vertical fish distributions and the depth of the oxic–anoxic interface in this region.

### Method applicability beyond the Gotland Basin

In the Western Gotland Basin, we have tracked the position of the hypoxic horizon by its tight correlation to the strong salinity-driven stratification in the water column. The ground truth stations show that this correlation holds true across the survey region; however, across the Baltic Sea and in other oceans and basins, the same tight correlation may not exist. In these situations, our method may still be applicable, though slightly modified, through the same linking process of acoustic profiles to ground truth stations.

One such region where a modified version of this method could be applied is in the Bornholm Basin, a region south of the study site described in this manuscript. The Bornholm Basin, like the Gotland Basin, is a region known for low-oxygen conditions (Feistel *et al.*, 2016). Unlike the Western Gotland Basin, however, anoxia is seasonal and the oxycline in the Gotland Basin has been shown to commence well below halocline (Hansson *et al.*, 2018), precluding a direct depth correlation between acoustic scattering and the hypoxic horizon. However, preliminary processing of CTD and broadband EK80 data from Bornholm shows that a strong scattering interface (driven by a combined thermocline and halocline) can be linked to the hypoxic horizon through a static offset (Supplementary Figure S26). In the Bornholm Basin, or other similar regions, strong and spatially contiguous pycnoclines can be tracked using the acoustic methods outlined in this manuscript; and with successful collection of ground truth data, it should be possible to successfully track an oxygen horizon, even without a direct depth correlation. Additional information on this application of the method can be found in the [Supplementary data](#).

Still, in other, more dynamic regions of the Baltic Sea and elsewhere, the methods in this manuscript may not be applicable. In areas with strong currents, tidal forcing, or other lateral advection events the water column structure can dramatically vary across short distances. Acoustically tracking a specific interface and linking it to an oxygen horizon could prove difficult in such an area, made more complicated by the potential for other types of scattering mechanism, such as turbulent microstructure or suspended sediment. The Southern Quark (Muchowski *et al.*, 2020) is a region of the Baltic Sea not well suited for this method; beyond the Baltic Sea, many estuaries would likely prove too dynamic for this method (Lavry *et al.*, 2013).

## Conclusions

In this work, we have shown that the permanent halocline in the Western Gotland Basin of the Baltic Sea can be tracked with broadband acoustics across large regions of the basin with vertical and horizontal resolutions on the order of meters and centimeters, respectively. Furthermore, when directly sampled at discrete stations, this stratification interface was successfully associated with a specific dissolved oxygen level, 2 ml/l, in the water column. This allowed for the remote identification and tracking of the oxic–anoxic interface throughout the basin.

The high-resolution maps produced through this work offer important new insights into the horizontal and vertical distribution of anoxic waters in the Gotland Basin. We identified that mixing, driven by double diffusion, and external forcing (e.g. wind-driven down-welling) are actively influencing the distribution of oxygen in the Gotland Basin. These observations, along with the high resolution map, would not have been possible to replicate with traditional point methods, which can fail to capture high-frequency spatial and temporal variability (e.g. CTD, moorings). Future efforts using these methods could provide more detailed information on the response of the anoxic zone to seasonal processes, major inflow events, and long-term forcing, such as the warming of the Baltic Sea.

As discussed above, this method, or a slightly modified form of this method, could be applied to other basins and regions within the Baltic Sea. Many research vessels associated with active Baltic Sea oxygen-monitoring programmes (e.g. HELCOM) are equipped with, or could be easily equipped with, active broadband sonar systems. In addition, long-term observation platforms (e.g. mooring, buoys) could be equipped with broadband acoustic packages and deployed to collect long-term acoustic time series. As the broadband acoustic methodology used in this work requires corresponding *in situ* measurements to provide both verification of the scattering mechanism responsible and dissolved oxygen levels in the water column, it would be possible to “upgrade” such vessel- and mooring-based monitoring programmes with this complementary acoustic method. The result would provide more accurate, higher-resolution maps, as exemplified in [Figure 5](#), to better inform the scientific community, governments, and public of the actively changing anoxic conditions in the Baltic Sea and beyond.

## Supplementary data

[Supplementary material](#) is available at the *ICESJMS* online version of the manuscript.

## Funding

BEAM (Baltic Sea Ecosystem Approach to Management) funded field work. Elizabeth Weidner, Thomas C. Weber, and Larry Mayer received support from NOAA grant NA15NOS400002000. Christian Stranne received support from the Swedish Research Council (Vetenskapsrådet, grant 2018-04350).

## Acknowledgements

The authors would like to thank the captain and crew of *RV Electra* and the Baltic Sea Centre for their support. All data are available from the authors upon request.

## References

- Anderson, V. 1950. Sound scattering from a fluid sphere. *Journal of the Acoustical Society of America*, 22: 426–431.
- Andrén, E., Andrén, T., and Kunzendorf, H. 2000. Holocene history of the Baltic Sea as a background for assessing records of human impact in the sediments of the Gotland Basin. *Holocene*, 10: 687–702.
- Bertrand, A., Ballón, M., and Chaigneau, A. 2010. Acoustic observations of living organisms reveals the upper limit of the oxygen minimum zone. *PLoS One*, 5: e10330.
- Blomberg, A. E. A., Weber, T. C., and Austeng, A. 2018. Improved visualization of hydroacoustic plumes using the split-beam aperture coherence. *Sensors*, 18: 2033.
- Camilli, R., Di Iorio, D., Bowen, A., Reddy, C. M., Techet, A. H., Yoerger, D. R., Whitcomb, L. L., *et al.* 2012. Acoustic measurement of the Deepwater Horizon Macondo well flow rate. *Proceeding of the National Academy of Sciences of the United States of America*, 109: 20235–20239.
- Carstensen, J., Andersen, J. H., Gustafsson, B. G., and Conley, D. J. 2014. Deoxygenation of the Baltic Sea during the last century. *Proceeding of the National Academy of Sciences of the United States of America*, 111: 5628–5633.
- Casini, M., Eero, M., Carlshamre, S., and Lövgren, J. 2016. Using alternative biological information in stock assessment: condition-corrected natural mortality of Eastern Baltic cod. *ICES Journal of Marine Science*, 73: 2625–2631.
- Clay, C. S., and Medwin, H. 1977. *Acoustical Oceanography: Principles and Applications*. John Wiley & Sons, Inc., New York. 2 pp.
- Conley, D. J., Björck, S., Bonsdorff, E., Carstensen, J., Destouni, G., Gustafsson, B. G., Hietanen, S., *et al.* 2009. Hypoxia-related processes in the Baltic Sea. *Environmental Science Technology*, 43: 3412–3420.
- Conley, D. J., Humborg, C., Rahm, L., Savchuk, O. P., and Wulff, F. 2002. Hypoxia in the Baltic Sea and basin-scale changes in phosphorus biogeochemistry. *Environmental Science Technology*, 36: 5315–5320.
- Diaz, R. J., and Rosenberg, R. 2008. Spreading dead zones and consequences for marine ecosystems. *Science*, 321: 926–929.
- Demer, D. A., Berger, L., Bernasconi, M., Bethke, E., Boswell, K., Chu, D., Domokos, R., Dunford, A., Fässler, S., Gauthier, S., Hufnagle, L. T., Jech, J. M., Bouffant, N., LeBourges-D’Haussy, A., Lurton, X., Macaulay, G. J., Perrot, Y., Ryan, T., Parker-Stetter, S., Stienessen, S., Weber, T. C., and Williamson, N. 2006. Calibration of acoustic instruments. *ICES Cooperative Research Report 326*. 133 pp. doi.org/10.17895/ices.pub.5494.
- Döös, K., Meier, H. E., and Döscher, R. 2004. The Baltic Haline conveyor belt or the overturning circulation and mixing in the Baltic. *Ambio*, 33: 261–266.
- Eby, L. A., and Crowder, L. B. 2002. Hypoxia-based habitat compression in the Neuse river estuary: context-dependent shifts in behavioral avoidance thresholds. *Canadian Journal of Fisheries Aquatic Science*, 59: 952–965.
- Ekau, W., Auel, H., Pörtner, H. O., and Gilbert, D. 2010. Impacts of hypoxia on the structure and processes in pelagic communities (zooplankton, macro-invertebrates and fish). *Biogeosciences*, 7: 1669–1699.
- Elken, J., Mälkki, P., Alenius, P., and Stipa, T. 2006. Large halocline variations in the Northern Baltic Proper and associated meso- and basin-scale processes. *Oceanologia*, 48: 91–117.
- EMODnet Bathymetry Consortium. 2018. EMODnet Digital Bathymetry (DTM). EMODnet Bathymetry Consortium, European Marine Observation and Data Network.
- Feistel, S., Feistel, R., Nehring, D., Matthäus, W., Nausch, G., and Naumann, M. 2016. Hypoxic and anoxic regions in the Baltic Sea, 1969–2015. *Meereswissenschaftliche Berichte: Marine Science Reports, Warnemünde*, 100.
- Fonselius, S., and Valderrama, J. 2003. One hundred years of hydrographic measurements in the Baltic Sea. *Journal of Sea Research*, 49: 229–241.
- Graham, L. P. 2004. Climate change effects on river flow to the Baltic Sea. *Ambio*, 33: 235–241.
- Hansson, M., Viktorsson, L., and Andersson, L. 2018. Oxygen survey in the Baltic Sea 2018: extent of anoxia and hypoxia, 1960–2018. *Report Oceanography 65*. <http://www.diva-portal.org/smash/record.jsf?pid=diva2%3A1314275&dsid=5915> (last accessed 10 August 2020).
- Hayes, H. C. 1924. Measuring ocean depths by acoustical methods. *Journal of the Franklin Institute*, 197: 323–354.
- Holtermann, P. L., Prien, R., Naumann, M., Mohrholz, V., and Umlauf, L. 2017. Deepwater dynamics and mixing processes during a major inflow event in the central Baltic Sea. *Journal of Geophysical Research: Oceans*, 122: 6648–6667.
- Hong, B., Swaney, D. P., Mörth, C. M., Smedberg, E., Hägg, H. E., Humborg, C., Howarth, R. W., *et al.* 2012. Evaluating regional variation of net anthropogenic nitrogen and phosphorus inputs (NANI/NAPI), major drivers, nutrient retention pattern and management implications in the multinational areas of Baltic Sea basin. *Ecological Model*, 227: 117–135.
- IOC, SCOR and IAPSO. 2010. The international thermodynamic equation of seawater – 2010: Calculation and use of thermodynamic properties. Intergovernmental Oceanographic Commission, Manuals and Guides 56, UNESCO (English). 196 pp.
- Kabel, K., Moros, M., Porsche, C., Neumann, T., Adolphi, F., Andersen, T. J., Siegel, H., *et al.* 2012. Impact of climate change on the Baltic Sea ecosystem over the past 1,000 years. *Nature Climate Change*, 2: 871–874.
- Lavery, A., Geyer, W. R., and Scully, M. E. 2013. Broadband acoustic quantification of stratified turbulence. *Journal of the Acoustical Society of America*, 134: 40–54.
- Lavery, A., and Ross, T. 2007. Acoustic scattering from double-diffusive microstructure. *Journal of the Acoustical Society of America*, 122: 1449–1462.
- Lavery, A., Schmitt, R. W., and Stanton, T. K. 2003. High-frequency acoustic scattering from turbulent oceanic microstructure: the importance of density fluctuations. *Journal of the Acoustical Society of America*, 114: 2685–2697.
- Lurton, X. 2010. *An Introduction to Underwater Acoustics*, 2nd edn. Springer-Verlag, Berlin/Heidelberg/Oxford. 680 pp.
- Meier, H. E. M., Feistel, R., Piechura, J., Arneborg, L., Burchard, H., Fiekas, V., Golenko, N., *et al.* 2006. Ventilation of the Baltic Sea deep water: a brief review of present knowledge from observation and models. *Oceanologia*, 48: 133–164.
- Merewether, R., Olsson, M. S., and Lonsdale, P. 1985. Acoustically detected hydrocarbon plumes rising from 2-km depths in the Guaymas Basin, Gulf of California. *Journal of Geophysical Research*, 90: 3075–3085.
- Mortimer, C. H. 1941. The exchange of dissolved substances between mud and water in lakes. *Journal of Ecology*, 29: 280–329.
- Muchowski, J., Umlauf, L., Arneborg, L., Weidner, E., Holtermann, P. L., Peng, J., Humborg, C., and Stranne, C., 2020. High-resolution turbulence observations of non-tidal stratified flow over a steep sill in the Baltic Sea. *In Proceedings of the Ocean Sciences Meeting 2020*, 16–21 February 2020, San Diego, CA. Abstract PS13A-07.
- Neuenfeldt, S. 2002. Influence of oxygen saturation on the distributional overlap of predator (cod, *Gadus morhua*) and prey (herring, *Clupea harengus*) in the Bornholm Basin of the Baltic. *Fisheries Oceanography*, 11: 11–17.
- Proni, J. R., and Apel, J. R. 1975. On the use of high-frequency acoustics for the study of internal waves and microstructure. *Journal of Geophysical Research*, 80: 1147–1151.

- Rabalais, N. N., Turner, R. E., Diaz, R. J., and Justic, D. 2009. Global change and eutrophication of coastal waters. *ICES Journal of Marine Science*, 66: 1528–1537.
- Rabalais, N. N., Turner, R. E., and Wiseman, W. J. 2002. Gulf of Mexico Hypoxia, A.K.A. “The Dead Zone”. *Annual Review of Ecological Systems*, 33: 235–263.
- Randell, D. J. 1970. *Fish Physiology: The Nervous System, Circulation, and Respiration*, pp. 253–292. Academic.
- Ross, T., and Lavery, A. 2012. Scattering from ocean pycnoclines. *Journal of the Acoustical Society of America*, 131: EL54–EL60.
- Ruddick, B., and Gargett, A. E. 2003. Oceanic double-diffusion: introduction. *Progress in Oceanography*, 56: 381–393.
- Schmale, O., Krause, S., Holtermann, P., Power Guerra, N. C., and Umlauf, L. 2016. Dense bottom gravity currents and their impact on pelagic methanotrophy at oxic/anoxic transition zones. *Geophysical Research Letters*, 43: 5225–5232.
- Shibley, N. C., Timmermans, M. L., Carpenter, J. R., and Toole, J. M. 2017. Spatial variability of the Arctic Ocean’s double-diffusive staircase. *Journal of Geophysical Research Oceans*, 122: 980–994.
- Simmonds, E. J., and MacLennan, D. N. 2005. *Fisheries Acoustics*, 2nd edn. Blackwell Publishing, Oxford. 437 pp.
- Smith, S. V., and Hollibaugh, J. T. 1989. Carbon-controlled nitrogen cycling in a marine “macrocosm”: an ecosystem scale model for managing coastal eutrophication. *Marine Ecology Progress Series*, 52: 103–109.
- Stramma, L., Johnson, G. C., Sprintall, J., and Mohrholz, V. 2008. Expanding oxygen-minimum zones in the tropical oceans. *Science*, 320: 655–658.
- Stranne, C., Mayer, L., Jakobsson, M., Weidner, E., Jerram, K., Weber, T. C., Anderson, L. G., *et al.* 2018. Acoustic mapping of mixed layer depth. *Ocean Science*, 14: 503–514.
- Stranne, C., Mayer, L., Weber, T. C., Ruddick, B. R., Jakobsson, M., Jerram, K., Weidner, E., *et al.* 2017. Acoustic mapping of thermohaline staircases in the Arctic Ocean. *Scientific Reports*, 7: 15192.
- Tait, R. I., and Howe, M. R. 1968. Some observations of thermohaline stratification in the deep ocean. *Deep-Sea Research*, 15: 275–280.
- Taylor, J. C., and Rand, P. S. 2003. Spatial overlap and distribution of anchovies (*Anchoa spp.*) and copepods in a shallow stratified estuary. *Aquatic Living Resources*, 16: 191–196.
- Timmermans, M. L., Toole, J. M., Krishfield, R., and Winsor, P. 2008. Ice-tethered profiler observations of the double-diffusive staircase in the Canada Basin thermocline. *Journal of Geophysical Research*, 113: C00A02.
- Turner, J. S. 1968. The behavior of a stable salinity gradient heated from below. *Journal of Fluid Mechanics*, 33: 183–200.
- Umlauf, L., Holtermann, P. L., Gillner, C. A., Prien, R. D., Merkelbach, L., and Carpenter, J. R. 2018. Diffusive convection under rapidly varying conditions. *Journal of Physical Oceanography*, 48: 1731–1747.
- Vaquar-Sunyer, R., and Duarte, C. M. 2008. Thresholds of hypoxia for marine biodiversity. *Proceedings of the National Academy of Sciences of the United States of America*, 105: 15452–15457.
- Viktorsson, L. 2017. Hydrography and oxygen in the deep basins, HELCOM Baltic Sea Environment Fact Sheets. <http://www.helcom.fi/baltic-sea-trends/environment-fact-sheets/> (last accessed 10 August 2020).
- Weidner, E., Weber, T. C., Mayer, L., Jakobsson, M., Chernykh, D., and Semiletov, I. 2019. A wideband acoustic method for direct assessment of bubble-mediated methane flux. *Continental Shelf Research*, 173: 104–115.
- Winsor, P., Rodhe, J., and Omstedt, A. 2001. Baltic Sea ocean climate: an analysis of 100 yr of hydrographic data with focus on the freshwater budget. *Climate Research*, 18: 5–15.
- Zillén, L., Conley, D. J., Andrén, T., Andrén, E., and Björck, S. 2008. Past occurrences of hypoxia in the Baltic Sea and the role of climate variability, environmental change and human impact. *Earth Science Review*, 91: 77–92.

*Handling editor: Roland Proud*